Solar constraints on new couplings between electromagnetism and gravity

S. K. Solanki,[1] O. Preuss,[1] M. P. Haugan,[2] A. Gandorfer,[1,3] H. P. Povel,[3] P. Steiner,[3] K. Stucki,[3]
P. N. Bernasconi,[4] and D. Soltau[5]

[1]*Max-Planck-Institut für Aeronomie, D-37191 Katlenburg-Lindau, Germany*
[2]*Department of Physics, Purdue University, 1396, West Lafayette, Indiana 47907, USA*
[3]*Institute of Astronomy, ETH-Zentrum, CH-8092 Zürich, Switzerland*
[4]*Space Department, Johns Hopkins University, Applied Physics Laboratory,*
11100 Johns Hopkins Road, Laurel, Maryland 20723-6099, USA
[5]*Kiepenheuer-Institut für Sonnenphysik, D-79104 Freiburg, Germany*

(Received 20 August 2003; published 11 March 2004)

The unification of quantum field theory and general relativity is a fundamental goal of modern physics. In many cases, theoretical efforts to achieve this goal introduce auxiliary gravitational fields, ones in addition to the familiar symmetric second-rank tensor potential of general relativity, and lead to nonmetric theories because of direct couplings between these auxiliary fields and matter. Here, we consider an example of a metric-affine gauge theory of gravity in which torsion couples nonminimally to the electromagnetic field. This coupling causes a phase difference to accumulate between different polarization states of light as they propagate through the metric-affine gravitational field. Solar spectropolarimetric observations are reported and used to set strong constraints on the relevant coupling constant k: $k^2 < (2.5\ \mathrm{km})^2$.

DOI: 10.1103/PhysRevD.69.062001 PACS number(s): 04.80.Cc, 04.50.+h, 96.60.Tf

I. INTRODUCTION

The quest for a complete and self-consistent unification of quantum field theory with the theory of general relativity remains one of the most important unsolved problems in modern theoretical physics. Its solution promises an extension of the standard model of particle physics that encompasses all fundamental interactions and accounts for everything from the evolution of the early Universe to black hole physics. This possibility continues to inspire work on such theories even after decades of effort. Clearly, one can expect candidate theories to predict *new physics*, that is, phenomena beyond the scope of general relativity and the standard model. The birefringence we study here is an example.

Quantum gravity research is unusual in that it is driven by the need to overcome extraordinary conceptual and mathematical difficulties in formulating a consistent theory rather than by an accumulation of experimental evidence that could inform one's choices among theoretical alternatives. Exploring such alternatives during the past several decades has produced many theories of gravity and, thus, a need for an overarching theoretical framework within which these alternatives can be compared and classified. The Dicke framework, defined in Appendix 4 of Dicke's 1964 Les Houches lectures [1], can be seen as the basis for a number of formalisms encompassing Lagrangian-based local field theories of gravity. It demands that gravity be associated with one or more fields of tensorial character. Consequently, alternatives to general relativity generally feature one or more gravitational fields in addition to the usual second-rank symmetric tensor potential. The distinction between metric and nonmetric alternatives often turns on the manner in which matter couples to such additional fields. The purely geometrical character of general relativity and other metric theories is a consequence of the familiar minimal coupling of matter fields to a single symmetric second-rank tensor gravitational field. Nonmetric theories deviate from this pattern, typically including direct couplings between matter and auxiliary gravitational fields. The Dicke framework encompasses nonmetric as well as metric theories of gravity and, therefore, general relativity as a particular example for a metric theory. In this paper we focus on observable consequences of a nonminimal coupling between a gravitational torsion field and the electromagnetic field.

An appropriate framework for the analysis of electrodynamics in a background gravitational field is given by the χg formalism, invented by Ni in 1977 [2]. The χ of its name refers to a tensor density which provides a phenomenological representation of gravitational fields. The structure of the χg formalism is in agreement with the basic assumptions and constraints of the Dicke framework. Demanding electromagnetic gauge invariance and linearity of the electromagnetic field equations, the most general Lagrangian density governing source-free electromagnetic field dynamics is

$$\mathcal{L}_{\mathrm{NG}} = -\frac{1}{16\pi}\chi^{\alpha\beta\gamma\delta}F_{\alpha\beta}F_{\gamma\delta}. \tag{1}$$

The independent components of the tensor density $\chi^{\alpha\beta\gamma\delta}$ comprise 21 phenomenological gravitational potentials that allow one to represent gravitational fields in a very broad class of nonmetric theories. Ni [3] noted that theories encompassed by this formalism can predict birefringence and used pulsar polarization observations to constrain this possibility. Perhaps because no specific theory predicting birefringence was recognized at that time, the significance of Ni's result was initially overlooked.

This situation changed when Moffat published a revised version of his nonsymmetric gravitation theory (NGT) [6]. One year later, Gabriel *et al*. showed that NGT predicts a polarization-dependent speed of light as a consequence of a violation of the Einstein equivalence principle and imposed

 ©2004 The American Physical Society

the first sharp constraints on the magnitude of this birefringence [7–9] (in this context see also Solanki and Haugan [4] and Solanki *et al.* [5]). In contrast to these earlier investigations, the present paper is not concerned with NGT. It focuses on another alternative to general relativity drawn from the class of metric-affine theories of gravity (MAG) [13], in part because an array of technical difficulties have challenged the viability of NGT [11,12]. We show that birefringence is a generic feature of MAG in the case of nonminimal coupling between electromagnetism and gravity, specifically torsion, and use solar data to set sharp constraints on a relevant coupling constant. We hope that this example will prompt further work on gravity-induced birefringence predicted by metric-affine theories and other alternatives to general relativity. In that regard, see [14,15].

It is important to note that the significance of such constraints goes far beyond testing versions of NGT or MAG. These are merely concrete examples of theories that predict gravity-induced birefringence, a phenomenon shown by Haugan and Kauffmann [10] to be predicted by a broad class of the nonmetric theories encompassed by the χg formalism. Here we make use of the formalism they invented to compute the effect of gravity-induced birefringence using the χg representation of any gravitational field. We emphasize that observations constraining the strength of such birefringence complement more familiar tests of the Einstein equivalence principle like the Eötvös, gravitational redshift and Hughes-Drever experiments, which currently do not bound our special nonminimal coupling. The reason is that we focus on a quite novel coupling between electromagnetic fields and torsion which was not taken into account in the analysis of these classical experiments. However, since our new coupling also violates local Lorentz invariance as one can see from Eq. (2), it is indeed thinkable that Eötvös, Hughes-Drever or redshift experiments could also constrain this new possibility.

We also report on new solar polarization data and the constraints on such gravity-induced birefringence obtained therewith. In Sec. III A we describe the new profile difference technique we use to search for evidence of birefringence. In Sec. III B we review the Stokes asymmetry technique proposed previously by Solanki and Haugan [4]. In Sec. IV we describe the solar data we analyze and the observations that produced them. The analysis of these data and the constraints we infer on gravity-induced birefringence are discussed in Sec. V. We quote constraints on the Sun's NGT charge, $l_{\odot}^2$, purely as a figure of merit that can be compared to prior constraints, but focus on constraints on a metric-affine parameter, k^2, defined in the next section.

II. GRAVITY-INDUCED BIREFRINGENCE IN METRIC-AFFINE THEORIES

An empirically adequate account of gravitation is given today by general relativity which predicts vanishing torsion and vanishing nonmetricity (covariant derivative of the metric). This account is, so far, in complete agreement with observational results. However, general relativity is a classical theory. The desire for a quantum mechanical account of gravitation requires a more general framework.

One possibility is to formulate gravity as a gauge theory of an underlying local spacetime group. Metric-affine gravity (MAG) is based on the assumption that affine transformations are the gauge group. It is the most general canonical gauge theory of gravity [13].

Metric-affine theories use a second-rank symmetric tensor field, a co-frame field and a connection one-form field to represent gravitational potentials. Although the symmetric tensor is referred to as the metric, metric-affine theories are generally nonmetric. Other gravitational potentials, specifically the torsion and nonmetricity fields extracted from the connection, couple directly to matter. Nonmetric couplings to the electromagnetic field can lead to gravity-induced birefringence.

In this section we will carefully examine the possible coupling of the electromagnetic field to gravity within the framework of MAG. Under the assumption of electric charge and magnetic flux conservation Puntigam *et al.* [16] showed that the conventional formulation of Maxwell-Lorentz electrodynamics in a metric-affine gravitational field predicts that the propagation of light is not influenced by the presence of post-Riemannian geometric fields like torsion T^{α} or nonmetricity $Q_{\alpha\beta}$. However, "admissible" nonminimal coupling possibilities that lead to birefringence do exist since one can modify the Maxwell-Lorentz spacetime relation $H = \lambda_0 \star F$. Couplings of this kind respect gauge invariance and, as a consequence, electric charge as well as magnetic flux conservation. In order to make quantitative predictions about electromagnetic field dynamics in a metric-affine background field using this nonminimal coupling scheme, a specific additional Lagrangian density is needed. We consider

$$L_{EM} = k^2 * (T_{\alpha} \wedge F) T^{\alpha} \wedge F, \tag{2}$$

consistent with the suppositions made above. Here, k is a coupling constant with units of length, * denotes the Hodge dual, T denotes the torsion and F the electromagnetic field. Our intention is to set strong limits on k^2 and, so, to decide about the physical relevance of the gravity-induced birefringence generated by the coupling (2). Currently there are no expectations from the theory side of what a reasonable value for k^2 might be. The additional Lagrangian (2) can be written as

$$\delta \mathcal{L}_{EM} = \delta \chi^{\alpha\beta\gamma\delta} F_{\alpha\beta} F_{\gamma\delta}, \tag{3}$$

so that we can make use of the general formalism developed by Haugan and Kauffmann in [10] to infer the consequences of the nonminimal coupling (2) on the propagation of light through a metric-affine field. This means that our objective is to compute the fractional difference in the propagation speed of linear polarization states

$$\frac{\delta c}{c} = \frac{1}{2} \sqrt{(\mathcal{A} - \mathcal{C})^2 + 4\mathcal{B}^2} \tag{4}$$

that are singled out by a solar torsion field. The coefficients $\mathcal{A}$, $\mathcal{B}$ and $\mathcal{C}$ depend on the location in spacetime and on the direction in which the wave propagates.

Since we are going to search for birefringence in the essentially static, spherically symmetric gravitational field of the Sun, we are interested in static and spherically symmetric solutions of the metric-affine field equations for torsion. One such solution was given by Tresguerres [17,18]. It can be split into nonmetricity dependent and independent parts. The latter, which is assumed to couple to the electromagnetic field via Eq. (2), is given by

$$T^{\alpha}=k_0\left[\frac{1}{r}(\theta^0-\theta^1)+\frac{m}{r^2}(\theta^0+\theta^1)\right]\wedge\theta^{\alpha}, \tag{5}$$

with torsion mass m and with $k_0=1$ for $\alpha=0,1$ or $k_0=-1/2$ for $\alpha=2,3$, respectively. In this equation we have dropped the dilatation charge N_0 from Tresguerres' original solution because it vanishes if the nonmetricity field does. Also the small observed value of the cosmological constant Λ means that effects of its term can be neglected on galactic and smaller scales.

Equation (5) is consistent with the most general static, spherically symmetric form for a torsion field [17]

$$T^0=\alpha(r)\,\theta^0\wedge\theta^1+\tilde{\alpha}(r)\,\theta^2\wedge\theta^3, \tag{6}$$

$$T^1=\beta(r)\,\theta^0\wedge\theta^1+\tilde{\beta}(r)\,\theta^2\wedge\theta^3, \tag{7}$$

$$T^2=\gamma_{(1)}\theta^0\wedge\theta^2+\gamma_{(2)}\theta^0\wedge\theta^3+\gamma_{(3)}\theta^1\wedge\theta^2+\gamma_{(4)}\theta^1\wedge\theta^3, \tag{8}$$

$$T^3=\gamma_{(1)}\theta^0\wedge\theta^3-\gamma_{(2)}\theta^0\wedge\theta^2+\gamma_{(3)}\theta^1\wedge\theta^3-\gamma_{(4)}\theta^1\wedge\theta^2. \tag{9}$$

The solution (5) is a special case having $\tilde{\alpha}(r)=\tilde{\beta}(r)=\gamma_{(2)}=\gamma_{(4)}=0$.

Plugging this general representation of a spherically symmetric torsion field into the Lagrangian density (2) yields

$$\begin{aligned}\delta\mathcal{L}_{EM}=k^2\{&(\alpha^2-\beta^2)B_1^2-(\gamma_{(1)}^2+\gamma_{(4)}^2)[B_2^2+B_3^2]\\&-(\gamma_{(3)}^2+\gamma_{(4)}^2)[E_2^2+E_3^2]\\&+2(\gamma_{(1)}\gamma_{(4)}-\gamma_{(2)}\gamma_{(3)})[B_2E_2+B_3E_3]\\&+2(\gamma_{(1)}\gamma_{(3)}+\gamma_{(2)}\gamma_{(4)})[B_3E_2-B_2E_3]\},\end{aligned} \tag{10}$$

where E and B refer in the usual way to the electric and magnetic components of F in Tresguerres' coordinates. Note that in his notation the three-vector index 1 refers to the radial direction. In terms of the components of the ξ, ζ and γ tensors of Ref. [10], the corresponding Lagrangian expression is

$$\begin{aligned}\delta\mathcal{L}_{EM}=&\zeta_{11}B_1^2+\zeta_{22}B_2^2+\zeta_{33}B_3^2-\xi_{22}E_2^2-\xi_{33}E_3^2\\&+2\{\gamma_{22}E_2B_2+\gamma_{33}E_3B_3+\gamma_{32}E_3B_2+\gamma_{23}E_2B_3\},\end{aligned} \tag{11}$$

from which the expressions for the nonzero components of the ξ, ζ and γ tensors in terms of Tresguerres' functions can be read for the nonminimal torsion coupling considered here. Haugan and Kauffmann [10] have shown that the expressions $\mathcal{A}-\mathcal{C}$ and $\mathcal{B}$ from Eq. (4) can now be expressed in terms of the spherical components of these tensors ξ, ζ and γ

$$\begin{aligned}\mathcal{A}-\mathcal{C}=\frac{2}{\sqrt{6}}[&(\xi^{(2)}_{2'}+\xi^{(2)}_{-2'})+2i(\gamma^{(2)}_{2'}-\gamma^{(2)}_{-2'})\\&+(\zeta^{(2)}_{2'}+\zeta^{(2)}_{-2'})]\end{aligned} \tag{12}$$

and

$$\begin{aligned}\mathcal{B}=-\frac{1}{\sqrt{6}}[&i(\xi^{(2)}_{2'}-\xi^{(2)}_{-2'})+2(\gamma^{(2)}_{2'}+\gamma^{(2)}_{-2'})\\&+i(\zeta^{(2)}_{2'}-\zeta^{(2)}_{-2'})].\end{aligned} \tag{13}$$

Only $l=2$ components appear. The m' notation indicates that these spherical components correspond to Cartesian components in a quasi-Lorentzian (t,x',y',z') coordinate system oriented so that the radiation of interest propagates in the z' direction. In the following, we exploit the fact that these spherical components can be expressed in terms of components in another quasi-Lorentzian (t,x,y,z) coordinate system via the familiar transformation law [19], e.g.

$$\xi^{(l)}_{m'}=\mathcal{D}^{(l)}_{m'm}(\phi,\theta,\psi)\,\xi^{(l)}_{m}, \tag{14}$$

where ϕ, θ and ψ are the Euler angles specifying the rotation from (t,x,y,z) to (t,x',y',z') and the rotation matrix $\mathcal{D}$ is given in terms of spherical harmonics.

Since the only direction that a spherical field can single out is the radial one, it is now useful to introduce, at each point along a light ray of interest, a local quasi-Lorentzian (t,x,y,z) coordinate system oriented so that the z axis is radial and the x axis lies in the ray's plane. This is convenient because the spherical tensors introduced above are simple in such local coordinate systems. Specifically, $\xi^{(2)}_m$, $\zeta^{(2)}_m$ and $\gamma^{(2)}_m$ are nonzero only for $m=0$.

At each point along the ray, the local (t,x,y,z) coordinate system is rotated about the y axis through an angle θ to obtain a local (t,x',y',z') system so that now the ray runs in the z' direction. The local value of $\delta c/c$ in Eq. (4) is expressed in terms of $\mathcal{A}-\mathcal{C}$ and $\mathcal{B}$ which are, in turn, expressed in terms of $\xi^{(2)}_{\pm2'}$, $\zeta^{(2)}_{\pm2'}$ and $\gamma^{(2)}_{\pm2'}$ according to Eqs. (12) and (13). Since the Euler angles of the rotation from (t,x,y,z) to (t,x',y',z') are θ and $\phi=\psi=0$, the transformation law (14) simplifies to

$$\xi^{(2)}_{\pm2'}=\sin^2\theta\,\xi^{(2)}_0, \tag{15}$$

with the same relationship between $\zeta^{(2)}_{\pm2'}$ and $\zeta^{(2)}_0$ and between $\gamma^{(2)}_{\pm2'}$ and $\gamma^{(2)}_0$. Here, θ denotes the angle between the light ray's propagation direction and the radial direction. Exploiting these transformations, Haugan and Kauffmann conclude from Eqs. (12) and (13) that

$$\mathcal{A}-\mathcal{C}=\frac{4}{\sqrt{6}}(\xi_0^{(2)}+\zeta_0^{(2)})\sin^2\theta \tag{16}$$

and

$$\mathcal{B}=-\frac{4}{\sqrt{6}}(\gamma_0^{(2)}\sin\theta)^2. \tag{17}$$

Substitution into Eq. (4) yields an expression for the fractional difference in the propagation speeds of linear polarization states for the case of a static spherically symmetric torsion field

$$\frac{\delta c}{c}=\sqrt{\frac{2}{3}}\sin^2\theta\sqrt{(\xi_0^{(2)}+\zeta_0^{(2)})^2+(4\gamma_0^{(2)})^2}. \tag{18}$$

To express this in terms of Tresguerres' parameters we simply use the relationship between the spherical and Cartesian components of ξ, ζ and γ and between those Cartesian components and Tresguerres' parameters,

$$\xi_0^{(0)}=\xi^{11}+\xi^{22}+\xi^{33}=2k^2(\gamma_{(3)}^2+\gamma_{(4)}^2)$$

$$\xi_0^{(2)}=\xi^{11}-\frac{1}{2}(\xi^{22}+\xi^{33})=-k^2(\gamma_{(3)}^2+\gamma_{(4)}^2)$$

$$\zeta_0^{(0)}=\zeta^{11}+\zeta^{22}+\zeta^{33}$$
$$=k^2[(\alpha^2-\beta^2)-2(\gamma_{(1)}^2+\gamma_{(2)}^2)]$$

$$\zeta_0^{(2)}=\zeta^{11}-\frac{1}{2}(\zeta^{22}+\zeta^{33})$$
$$=k^2[(\alpha^2-\beta^2)+(\gamma_{(1)}^2+\gamma_{(2)}^2)]$$

$$\gamma_0^{(0)}=\gamma^{11}+\gamma^{22}+\gamma^{33}$$
$$=2k^2(\gamma_{(1)}\gamma_{(3)}-\gamma_{(2)}\gamma_{(4)})$$

$$\gamma_0^{(2)}=\gamma^{11}-\frac{1}{2}(\gamma^{22}+\gamma^{33})$$
$$=-k^2(\gamma_{(1)}\gamma_{(4)}-\gamma_{(2)}\gamma_{(3)}).$$

For the particular torsion field (5) we have $\gamma_{(2)}=\gamma_{(4)}=0$ and, therefore, $\mathcal{B}=0$. Using Eq. (5) one gets

$$\xi_0^{(2)}=-\frac{k^2}{4}\left(\frac{1}{r^2}-\frac{2m}{r^3}+\frac{m^2}{r^4}\right) \tag{19}$$

$$\zeta_0^{(2)}=-\frac{4k^2m}{r^3}+\frac{k^2}{4}\left(\frac{1}{r^2}+\frac{2m}{r^3}+\frac{m^2}{r^4}\right) \tag{20}$$

which yields

$$\xi_0^{(2)}+\zeta_0^{(2)}=-\frac{3k^2m}{r^3} \tag{21}$$

so that we have

$$\mathcal{A}-\mathcal{C}=-\frac{12k^2m}{\sqrt{6}r^3}\sin^2\theta. \tag{22}$$

Therefore, the fractional difference between the velocities of the two polarization states is given by

$$\frac{\delta c}{c}=-\sqrt{6}\frac{k^2m}{r^3}\sin^2\theta, \tag{23}$$

where θ again denotes the angle relative to the outward radial direction in which the light is propagating. For the total phase shift $\Delta\Phi$ which accumulates between the source and the observer one now has to calculate

$$\omega\int\frac{\delta c}{c}dt=-\sqrt{6}\omega k^2m\int\frac{\sin^2\theta}{r^3}dt. \tag{24}$$

Recapitulating the analysis performed in [7,8], we find

$$\Delta\Phi=\sqrt{\frac{2}{3}}\frac{2\pi k^2m}{\lambda R^2}\frac{(\mu+2)(\mu-1)}{\mu+1}, \tag{25}$$

where μ denotes the cosine of the light source's heliocentric angle, λ is the light's wavelength and R is the Sun's radius.

III. TECHNIQUE

We follow two strategies to test for gravitational birefringence. One of these was outlined by Solanki and Haugan (1996) [4], but could not be applied due to a lack of appropriate data. It is summarized and its implementation is described in Sec. III B. The other technique is new and is described in Sec. III A. In order to compare the effectiveness of these techniques with results of previous attempts to set limits on gravity-induced birefringence, which dealt with NGT, we also briefly consider NGT here in addition to metric-affine theories of gravity.

A. Profile difference technique

This technique relies on the fact that $\Delta\Phi$ is expected to be a strong function of μ, which is confirmed in the two concrete cases of NGT (see Ref. [9]) and metric-affine theories (see Sec. II). $\Delta\Phi$ is the phase shift which accumulates as light propagates from a point on the solar surface to the observer between net circular polarization, described by the Stokes parameter V, and net linear polarization aligned at 45° to the nearest part of the solar limb, generally ascribed to Stokes U. Formulas for $\Delta\Phi$ as predicted by metric-affine theories are given in Sec II. For Moffat's NGT [6] a corresponding expression has been published by Gabriel *et al.* [7,9]. This means that for any sufficiently large NGT charge $\ell_\odot$ or equivalent metric-affine parameter k a mixture of Stokes V and U profiles will be observed from sources of polarization distributed across the solar disk (i.e. as a function of μ), irrespective of the exact polarization state of the emitted radiation (i.e. which mixture of V and U is produced at the solar surface). Let the subscripts "src" and "obs" signify the Stokes profiles as created at the source and as

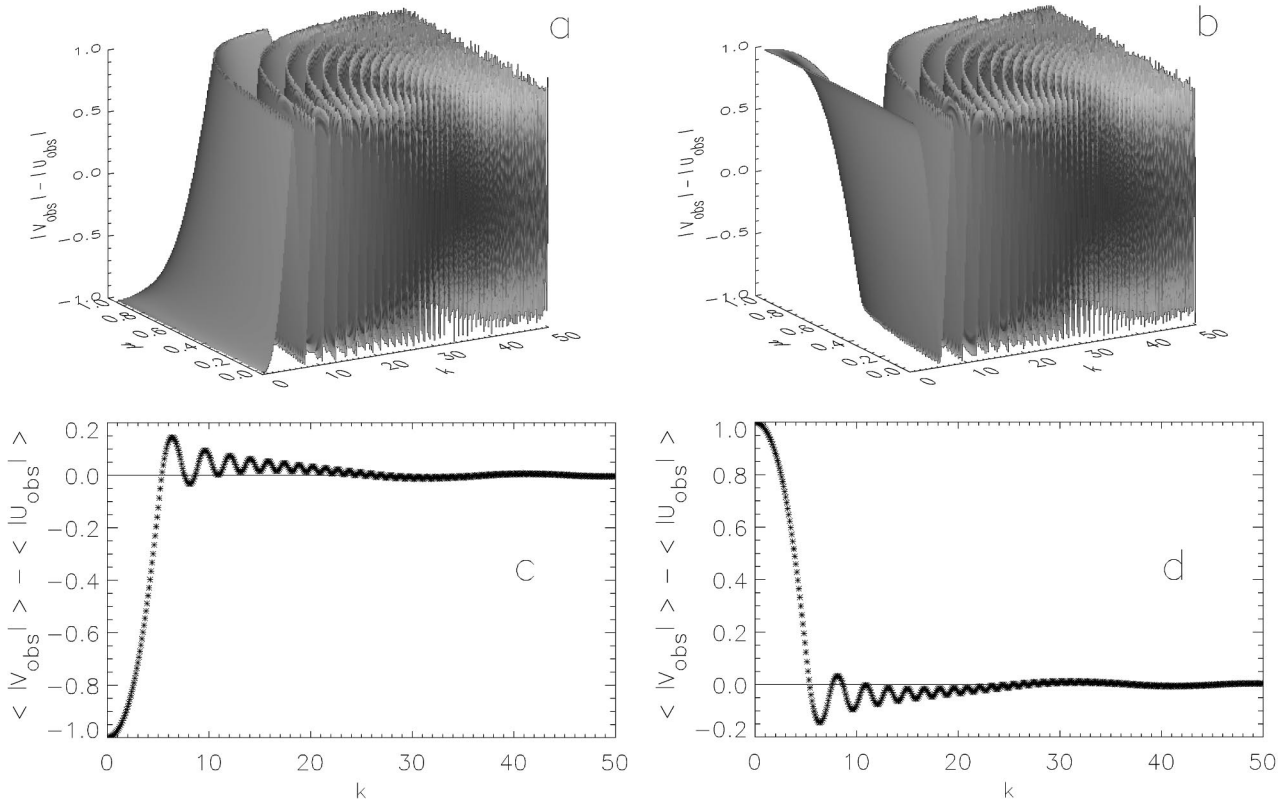

FIG. 1. Top: $|V_{obs}|-|U_{obs}|$ vs k and μ for $|V_{src}|=0$ (a) and $|U_{src}|=0$ (b). Bottom: $|V_{obs}|-|U_{obs}|$ averaged over all μ for the above cases.

observed, respectively. Then, irrespective of the value of $\langle|V_{src}|\rangle-\langle|U_{src}|\rangle$ for sufficiently large $\ell_\odot$ or k, $\langle|V_{obs}|\rangle-\langle|U_{obs}|\rangle$ will tend to zero. The averaging is over all μ values and the total number of profiles is assumed to be large.

This effect is illustrated in Fig. 1. In Figs. 1(a) and 1(b) $|V_{obs}|-|U_{obs}|$ is plotted vs k and μ for the extreme cases $|V_{src}|=0$ [Fig. 1(a)] and $|U_{src}|=0$ [Fig. 1(b)]. Other combinations of $|V_{src}(\mu)|$ and $|U_{src}(\mu)|$ give qualitatively similar results. The $|V_{obs}|-|U_{obs}|$ surface oscillates ever more rapidly with increasing k and with decreasing μ. Lines of equal $|V_{obs}|-|U_{obs}|$ are strongly curved in the k-μ plane. These two points combine to lead to decreasing $\langle|V_{obs}|\rangle-\langle|U_{obs}|\rangle$ with increasing k. This is shown in Figs. 1(c) and 1(d) for the cases illustrated in Figs. 1(a) and 1(b), respectively. As expected, the $\langle|V_{obs}|\rangle-\langle|U_{obs}|\rangle$ vs k curves exhibit a rapidly damped oscillation around zero. This effect can be used to set upper limits on gravitational birefringence if the observations exhibit a $\langle|V_{obs}|\rangle-\langle|U_{obs}|\rangle$ that differs significantly from zero. As we show later in this paper, this is indeed the case.

B. Stokes asymmetry technique

The strategy proposed by Solanki and Haugan [4] makes use of the symmetry properties of the Stokes profiles produced by the Zeeman splitting of atomic spectral lines. In the absence of radiative transfer effects in a strongly dynamic medium, net circular polarization, Stokes V, is antisymmetric in wavelength, and net linear polarization aligned at 45° to the solar limb, Stokes U, is symmetric. Birefringence, predicted by metric-affine gravity theories (and NGT) changes the phase between orthogonal linear polarizations and thus partly converts Stokes V into Stokes U and vice versa. However, U produced from V by gravitational birefringence still has the symmetry of V and can thus be distinguished from the Zeeman signal.

Let subscripts "a" and "s" signify the antisymmetric and symmetric parts of the Stokes profiles, respectively. Then,

$$\frac{U_{a,src}}{U_{s,src}}=\frac{V_{a,obs}\sin\Delta\Phi+U_{a,obs}\cos\Delta\Phi}{V_{s,obs}\sin\Delta\Phi+U_{s,obs}\cos\Delta\Phi}, \tag{26}$$

$$\frac{V_{s,src}}{V_{a,src}}=\frac{V_{s,obs}\cos\Delta\Phi+U_{s,obs}\sin\Delta\Phi}{V_{a,obs}\cos\Delta\Phi+U_{a,obs}\sin\Delta\Phi}. \tag{27}$$

Thus for observed symmetric and antisymmetric fractions of U and V Eqs. (3.1) and (27) predict the ratios U_a/U_s and V_s/V_a at the solar source.

If the solar atmosphere were static these ratios would vanish ($U_{a,src}=V_{a,src}=0$), so that any observed U_a or V_s would be due to either $\Delta\Phi$ or noise: $U_{a,obs}=V_{a,src}\sin\Delta\Phi$, $V_{s,obs}=U_{s,src}\sin\Delta\Phi$. The solar atmosphere is not static, however, and consequently the Stokes profiles do not fulfill the symmetry properties expected from the Zeeman effect even for rays coming from solar disk center ($\mu=1$), which are unaffected by gravitational birefringence. This asymmetry has been extensively studied, in particular for Stokes V, which most prominently exhibits it [20–22,24]. Although most pro-

files have $V_s/V_a \lesssim 0.2$, a few percent of V profiles exhibit V_s/V_a values close to unity, even at $\mu=1$. Such profiles occur in different types of solar regions, e.g. the quiet Sun [22], active region neutral lines [25] and sunspots [26]. The magnitude of V_s/V_a decreases rapidly with increasing V_a and profiles with $V_s/V_a \gtrsim 1$ are all very weak. They are often associated with the presence of opposite magnetic polarities within the spatial resolution element and a magnetic vector that is almost perpendicular to the line of sight, situations which naturally give rise to small V [26,27].

The observed Stokes U asymmetry is on average smaller than the V asymmetry. This is true in particular for extreme asymmetric values, i.e. $(U_{a,obs}/U_{s,obs})_{max} \ll (V_{s,obs}/V_{a,obs})_{max}$. Since this relation also holds at $\mu=1$ it is valid for source profiles as well. Thus, Sánchez Almeida and Lites [26] point out that Stokes U retains $U_{a,obs}/U_{s,obs} \ll 1$ throughout a sunspot, although $V_s/V_a > 1$ is invariably achieved at the neutral line. The reason for the smaller maximum asymmetry lies in the fact that Stokes U senses the transverse magnetic field. Since velocities in the solar atmosphere are directed mainly along the field lines they generally have a small line-of-sight component when U has a significant amplitude. Sizable line-of-sight velocities are needed, however, to produce a significant asymmetry [21]. Another reason for the smaller maximum U asymmetry is that, unlike Stokes V, it does not distinguish between oppositely directed magnetic fields.

Thus it is not surprising that in the following analysis Stokes U provides tighter limits than Stokes V. Another reason is that due to the on average stronger observed V profiles, asymmetries introduced in U (through gravitationally introduced cross-talk from V) are larger than the other way round. However, we also analyze Stokes V as a consistency check.

In order to separate the asymmetry produced by solar effects from that introduced by gravitational birefringence, one strategy to follow is to consider large amplitude Stokes profiles only. Another is to analyze data spanning a large range of μ values, since $\Delta\Phi$ exhibits a definite μ dependence. Finally, the larger the number of analyzed line profiles, the more precise the limit that can be set on $\Delta\Phi$. Better statistics not only reduce the influence of noise, they are also needed because for a single profile gravitational birefringence can both increase or decrease V_s/V_a and U_a/U_s. The latter may become important if the source profiles are strongly asymmetric. Thus a small observed V_s/V_a or U_a/U_s is in itself no guarantee for a small gravitational birefringence. However, since almost all source profiles are expected to have $V_s/V_a \ll 1$, $U_a/U_s \ll 1$, on average we expect gravitational birefringence to increase these ratios.

IV. OBSERVATIONS AND DATA

Two sets of data have been analyzed in the present paper. They are described below.

A. Data obtained in 1995

Observations were carried out from the 7–13th of November, 1995 with the Gregory Coudé Telescope (GCT) at the Teide Observatory on the Island of Tenerife. For the polarimetry we employed the first version of the Zürich Imaging Polarimeter (ZIMPOL I), which employs 3 CCD cameras, one each to record Stokes $I \pm Q$, $I \pm U$ and $I \pm V$ simultaneously [28].

The recorded wavelength range contains four prominent spectral lines, Fe I 5247.06 Å, Cr I 5247.56 Å, Fe I 5250.22 Å and Fe I 5250.65 Å. Three of these spectral lines are among those with the largest Stokes amplitudes in the whole solar spectrum and are also unblended by other spectral lines [29]. Blending poses a potentially serious problem since it can affect the blue-red asymmetry of the Stokes profiles. By analyzing more than one such line it is possible to reduce the influence of hidden blends and noise. Nowhere else in the visible spectrum are similar lines located sufficiently close in wavelength that they can be recorded simultaneously on a single detector. Also, compared to other lines with large Stokes amplitudes the chosen set lies at a short wavelength. This enhances $\Delta\Phi$ since it scales with $1/\lambda$. The sum of the above properties make the chosen range uniquely suited for our purpose.

In order to image all 4 spectral lines of interest onto a single CCD we introduced reduction optics between the image plane of the spectrograph and the detectors. They produce an image-scale reduction by a factor of 3.2. The final spectral resolving power $\lambda/\Delta\lambda$ corresponded to 210 000. The spatial scale corresponding to a pixel was 1.13 arcsec (or 860 km on the Sun). However, the effective spatial resolution of the data is limited by turbulence in the Earth's atmosphere, so-called ''seeing.'' This varied somewhat in the course of the observing run, so that the estimated angular resolution of the observations lies between 2.2 and 3 arcsec.

The modulator package, composed of 2 photoelastic modulators oscillating at frequencies of around 41 kHz and 42 kHz followed by a Glan linear polarizer, was placed ahead of the entrance slit to the spectrograph, but was nevertheless (unavoidably) located after 2 oblique reflections in the telescope. Oblique reflections produce cross-talk between Stokes parameters, i.e. they partially convert one form of polarization into another. Since we are trying to observe, or at least set limits on ''cross-talk'' between Stokes U and V due to gravitational birefringence we took some trouble to reduce the instrumental cross-talk to the extent possible. A first step was the choice of the telescope. With only two oblique reflections, whose relative angles change only slowly in the course of a year, the GCT is relatively benign compared to most other large solar telescopes. Secondly, a half-wave plate was introduced between the two oblique reflections. Sánchez Almeida *et al.* [30,31] have pointed out that a half-wave plate at that location should, under ideal circumstances, completely eliminate all instrumental cross-talk. To test the efficiency of the half-wave plate in suppressing instrumental cross-talk between Stokes Q, U and V we first carried out a series of observations of a sunspot near the center of the solar disk both with and without a half-wave plate introduced in the light path. Such tests were necessary since the half-wave plate available at the GCT is not optimized for the observed wavelength. Note that at solar disk center ($\mu=1$) $\Delta\Phi=0$, so that we test for instrumental

cross-talk only. The half-wave plate was indeed found to significantly reduce instrumental cross-talk. Remaining cross-talk was removed during data reduction using a numerical model of the telescope that includes an imperfect half-wave plate (adapted from a model kindly provided by Martínez Pillet). The parameters of the model were adjusted slightly using the observations of a sunspot umbra located close to $\mu=1$. We estimate that the residual cross-talk after this procedure is at the level of a few percent. Since Stokes V, Q, U profiles generally have amplitudes of $0.1I_c$ or less, the influence of the cross-talk is of the same order as the noise, which is roughly $(1-2)\times10^{-3}I_c$, where I_c is the continuum intensity. Photon noise is by far the largest contributor to this noise level. At this level instrumental cross-talk ceases to be of concern for our analysis.

The ZIMPOL polarimeters are unique in that they combine CCD detectors with a very high modulation frequency ($\geqslant$40 kHz) and hence preclude distortion of the Stokes profiles and cross-talk between them due to seeing fluctuations. The other advantage of the ZIMPOL working principle is the fact that the fractional polarization is absolutely free from gain-table or flat field noise [28]. This again improves the accuracy of the profile shapes and hence the reliability of our results.

A total of 106 recordings were made at different locations on the solar disk in an attempt to cover a large range of μ homogeneously. Particular emphasis was placed on observations close to the limb since gravitational birefringence is expected to be largest for such rays.

Since only a single sunspot was present on the solar disk during the observing run most recordings refer to faculae and network features, i.e. magnetic features with lower Stokes Q, U, V signals. In Fig. 2 a sample Stokes I,Q,U,V spectrum of a facular region near the solar limb is plotted. The 4 analyzed spectral lines are identified. These data were fully reduced following the tedious, but well-tested procedures described by Bernasconi [32].

B. Data set of March 2000

In order to improve the statistics and the μ coverage a second observing run was carried out in March 2000 with the Gregory-Coudé Telescope of IRSOL (Istituto Ricerche Solari Locarno) in Locarno, Switzerland. This telescope is almost identical to the GCT on Tenerife and the parameters such as spectral resolution, noise level etc. are very similar to those of the 1995 observations.

The next generation, ZIMPOL II polarimeter [33,34] was employed for the polarization analysis and data recording. It simultaneously records three of the four Stokes parameters, either Stokes I,Q,V or I,U,V on a single CCD detector chip. Observations in these two modes were interlaced, such that alternate exposures record Stokes I,Q,V and I,U,V, respectively. Exposures of the same Stokes parameters were then added together to reduce noise. Thus the final data set consists of all four Stokes parameters. The only differences with respect to the recordings made in 1995 are that the number of spatial pixels is reduced and that the noise level of Stokes V in the newer data is a factor of $\sqrt{2}$ lower than of Stokes Q and U, whereas Stokes Q, U and V had the same noise level in the earlier recordings. Due to the superior modulation scheme implemented in ZIMPOL II, Stokes Q and U achieve a noise level of $10^{-3}I_c$ after roughly the same exposure time during the observations made in 2000 as during the earlier campaign.

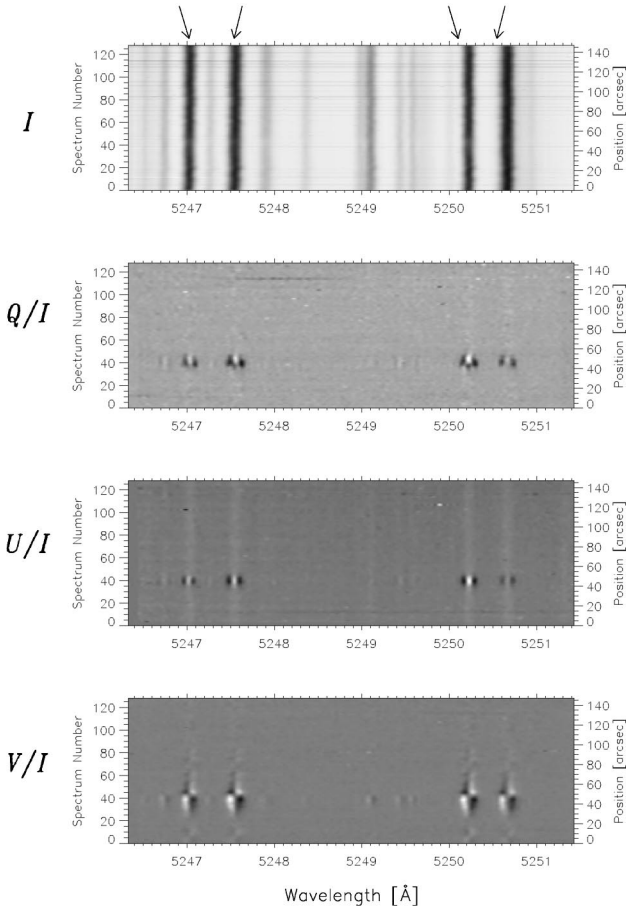

FIG. 2. Sample spectrum of Stokes I,Q,U and V.

These observations were carried out on the day of the equinox, at which time the two mirrors producing oblique reflections of the beam ahead of the modulator package are oriented such that their polarization cross-talk cancels out. Hence for these observations the instrumental cross-talk is essentially zero and no further treatment of the data for this effect is required.

The Sun was very active at the time of these observations with many active regions harboring sunspots and faculae present on the solar disk. Since active regions generally give larger amplitude Stokes signals we concentrated on observing them. A total of 7 exposures were made. The typical seeing during these observations was estimated to be 2–3 arcsec, while the spatial pixel size was 1.13 arcsec.

V. DATA ANALYSIS

Each exposure gives us the profiles of the 4 analyzed spectral lines in Stokes I,Q,U and V at a set of 94 (128 in the 1995 data) positions on the solar disk. Once the reduction and calibration procedure is completed we select from a given frame those spectra for further analysis for which the

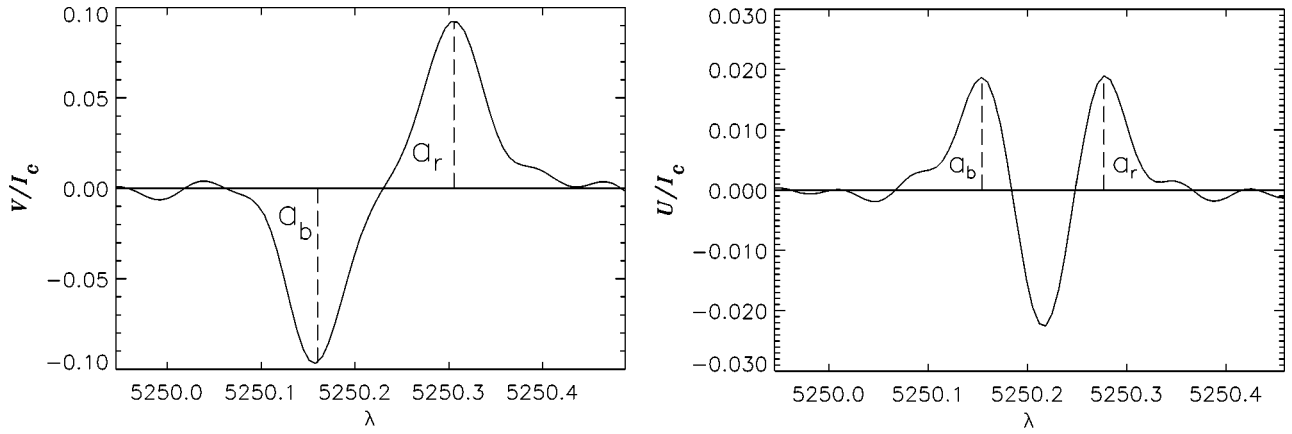

FIG. 3. Simultaneously measured profiles of Stokes V and Stokes U of the Fe I line at 5250.22 Å.

S/N ratio for either Stokes U or V in at least one of the four spectral lines is above 12 in the 1995 data and above 15 in the 2000 data.

This criterion gave us a total of 4480 profiles for further analysis. A nonorthogonal wavelet-packets smoothing scheme was employed to enhance the S/N ratio by a factor of 1.5–2 without significantly affecting the profile shapes [35].

Then the signed amplitudes of the blue and red wings, a_b and a_r (i.e. of the blue and red Zeeman σ-component) of all Stokes profiles of all 4 spectral lines were determined. In Fig. 3 we plot observed Stokes U and V profiles of the Fe I line at 5250.22 Å. $a_{b,r}(V)$ and $a_{b,r}(U)$ are indicated in the figure. Using these we can form the symmetric and antisymmetric parts of the Stokes V and U profile amplitudes, $V_s=(a_b+a_r)/2$, $V_a=(a_b-a_r)/2$, $U_s=(a_b+a_r)/2$ and $U_a=(a_b-a_r)/2$, respectively, which enter Eqs. (26) and (27). In the following all V and U values and parameters are normalized to the continuum intensity, even when not explicitly mentioned.

A. Profile difference analysis

We now apply the technique outlined in Sec. III A to our data. Due to the limited number of profiles and their irregular distribution over μ (see Sec. V B) any limit on gravitational birefringence will be less tight than what is achievable with ideal data presented in Sec. III A. In Fig. 4 we plot

$$\frac{|\langle|V_{\rm obs}|\rangle-\langle|U_{\rm obs}|\rangle|}{\langle|V_{\rm obs}|\rangle+\langle|U_{\rm obs}|\rangle} \quad \text{vs } k, \tag{28}$$

for different initial phase differences $\Delta\Phi$ between the orthogonal modes of line Fe I 5250.65 Å. The averaging has been done over the μ values at which observations are available. This line is chosen, since it gives the tightest limits on k. The thick horizontal line represents the value obtained from observations. Obviously above $k^2=(13.8\ \text{km})^2$ the curve obtained from theory always lies below the observed value, hence ruling out such k values.

For comparison with literature values it is useful to set limits on the $\ell_\odot$-parameter in Moffats NGT, since earlier work has concentrated on constraining this theory. Using the profile difference technique we obtain $\ell_\odot^2<(178\ \text{km})^2$ measured in the line Fe I 5250.65 Å, compared with the previous tightest upper limit of $(305\ \text{km})^2$.

B. Stokes asymmetry technique

A measure of the asymmetry of a Stokes profile is given by the ratio $\delta V=V_s/V_a$, respectively $\delta U=U_a/U_s$ [20,24]) In Fig. 5 we plot these quantities vs $|V_a|$ and $|U_s|$, respectively. Each point in these plots refers to a Stokes profile of the Fe I 5250.65 Å line.

Although our observations cover a range of μ values, Fig. 5 is similar to corresponding figures based on data obtained near $\mu=1$ [23,24], where the influence of gravitational birefringence vanishes for symmetry reasons. For large amplitudes (V_a, U_s) the relative asymmetry (V_s/V_a, U_a/U_s) is small, while for weaker profiles it shows an increasingly

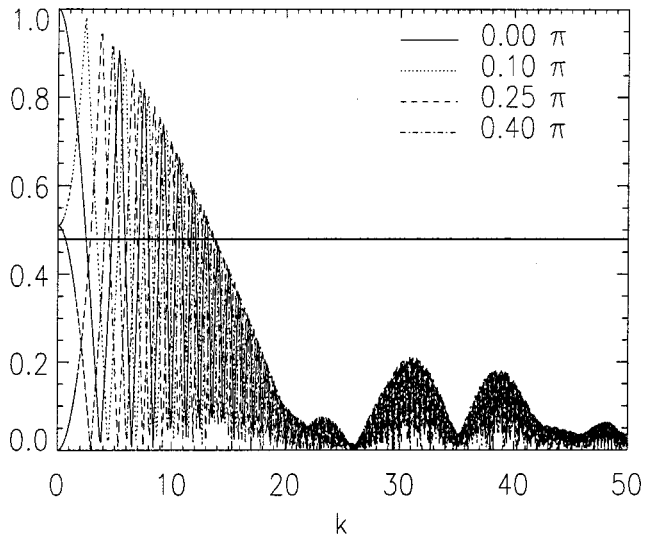

FIG. 4. The observable (Stokes V, Stokes U) mixture for initial phase differences of 0π, 0.1π, 0.25π and 0.4π plotted vs MAG coupling constant k. The horizontal solid line represents the value obtained from observations. Note that $\Delta\Phi$ values bigger than 0.5π give cyclic results.

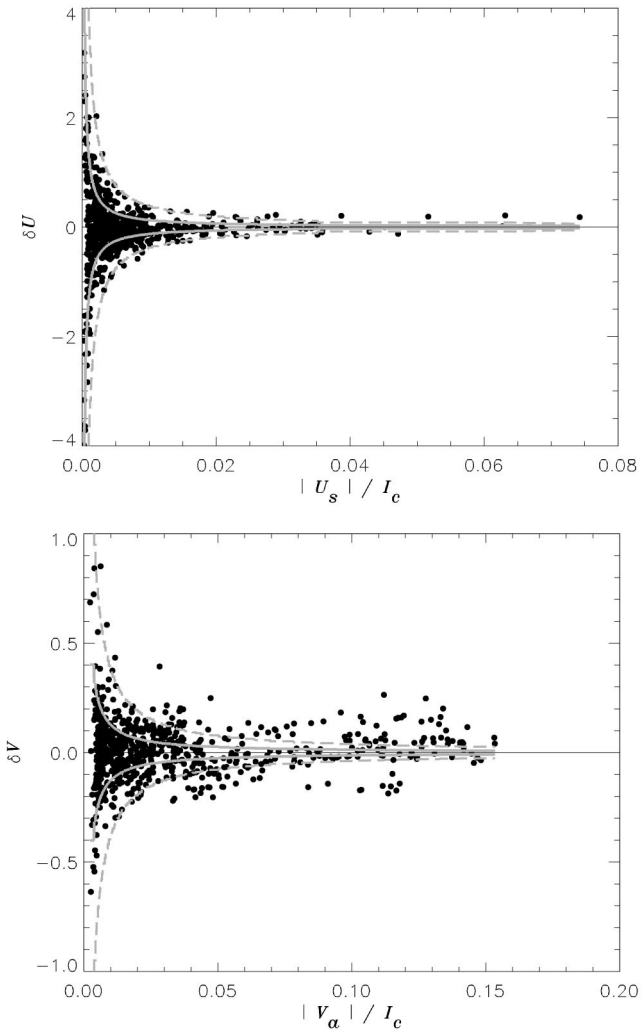

FIG. 5. Measured amplitude asymmetries for Stokes U and Stokes V.

large spread. For the weaker profiles this spread is mainly due to noise as can be judged from the solid and dashed curves in Fig. 5, which outline the 1σ and 3σ spread expected due to photon noise, respectively. The curves reveal that Stokes profiles with amplitudes (V_a, U_s) smaller than one percent of the continuum intensity are so strongly affected by noise that they are of little use for the present purpose. This leaves us with 1966 individual profiles for further analysis. In Fig. 6 we plot a histogram of the number of these profiles as a function of μ. The distribution is uneven, being determined by the position on the solar disk of magnetic features at the times of the observations.

The further analysis is made more complicated by the fact that a V_s and a U_a signal can be produced not just by gravitational birefringence, but also by radiative transfer processes acting in the dynamic solar atmosphere, as described in Sec. III. To circumvent this problem we consider all profiles satisfying the criterion that $|V_a|$ or $|U_s| \geq 0.01$. For all these profiles $|\delta V_{obs}| < 0.7$ and $|\delta U_{obs}| < 0.6$. A similar picture is also obtained at $\mu = 1$. Hence one way to limit k^2 is to require $|\delta V_{src}| < 1$ and $|\delta U_{src}| < 1$ for all μ. This condition is

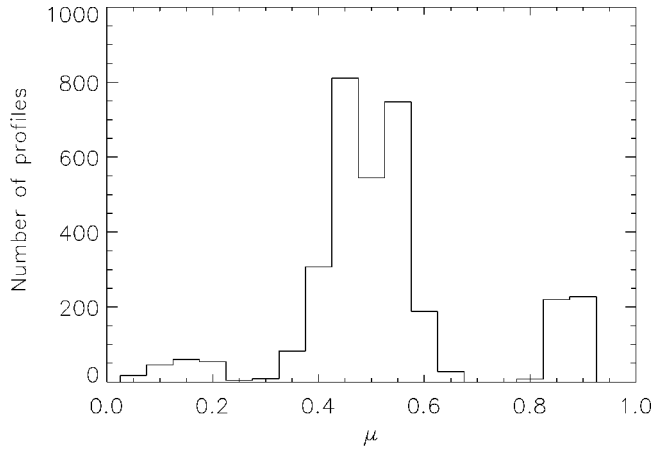

FIG. 6. Histogram of the number of recorded profiles as a function of μ.

strengthened by the fact that $|\delta V_{obs}|$ and $|\delta U_{obs}|$ decrease with decreasing μ [24,36], whereas gravitational birefringence increases towards the limb, so that one would expect exactly the opposite behavior if gravitational birefringence had a significant effect on the Stokes V or U profiles.

In Fig. 7 we plot the maximum $(U_{a,src}/U_{s,src})$ value predicted for each of the 4 spectral lines, based on all analyzed data, vs k^2. The horizontal line represents $\log(U_{a,src}/U_{s,src} = 1)$, a limit above which this ratio is not observed at $\mu \approx 1$. Clearly, as k^2 increases $(U_{a,src}/U_{s,src})_{max}$ initially remains almost equal to $(U_{a,obs}/U_{s,obs})_{max}$, but begins to increase for $k^2 \gtrsim (1\ \mathrm{km})^2$, becoming $\gtrsim 10$ at $k^2 < (2\ \mathrm{km})^2$ and finally oscillating around $(U_{a,src}/U_{s,src})_{max}$ of 100–1000. All 4 spectral lines exhibit a similar behavior, implying that the influence of noise is very small. The largest effect of gravitational birefringence is exhibited by the two most strongly Zeeman split lines, Cr I 5247.56 Å, Fe I 5250.22 Å, which also produce the largest Stokes V and U signals, while the lines with the smallest splitting, Fe I 5250.65 Å provide the weakest limit.

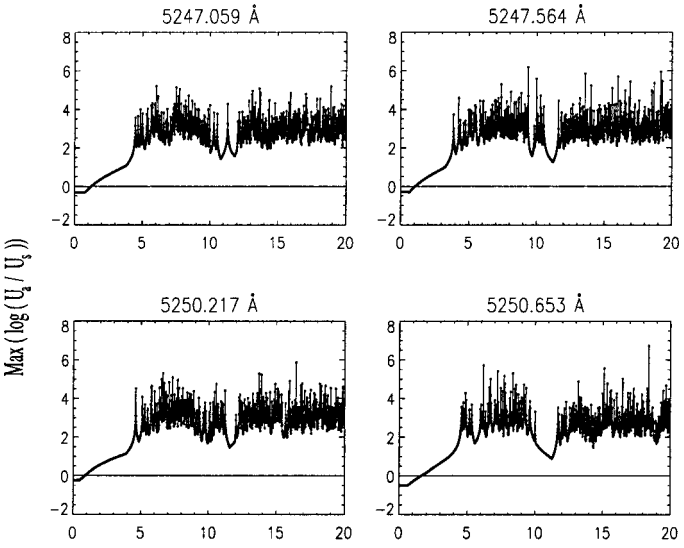

FIG. 7. Maximum of $(U_{a,src}/U_{s,src})$, on a logarithmic scale, values for all 4 spectral lines vs k.

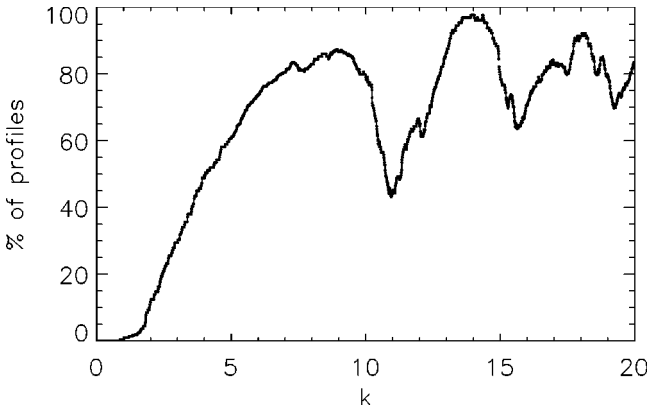

FIG. 8. Fraction of profiles with $(U_{a,src}/U_{s,src})>1$ for MAG.

It is in principle sufficient to limit k by requiring that none of the observed spectral lines has $(U_{a,src}/U_{s,src})>1$ within the range of allowed k values. This gives $k^2<(0.9\ \mathrm{km})^2$. A limit obtained similarly from Stokes V is both larger $k^2<(3.42\ \mathrm{km})^2$ and less reliable, since we cannot completely rule out $V_{s,src}/V_{a,src}>1$ to be present, although we expect such profiles to be very rare, among large amplitude profiles.

For Moffat's NGT this technique gives $\ell_\odot^2<(57{,}1\ \mathrm{km})^2$, implying a 28-fold reduction in $\ell_\odot^2$ compared to previous work.

An alternative test is to determine the fraction of profiles with $(U_{a,src}/U_{s,src})>1$ (Fig. 8). Figure 8 reveals that initially no U profile satisfies the criterion; above $k_\odot^2=(1.33\ \mathrm{km})^2$, 1.7% of the profiles does. This number keeps increasing with k, before finally oscillating around 70% at large k. Thus 10% of all data points have $(U_{a,src}/U_{s,src})>1$ for $k^2=(1.955\ \mathrm{km})^2$, 20% for $k^2=(2.43\ \mathrm{km})^2$. We are not aware of any solar observations of Stokes U with $\delta U>1$ for which instrumental cross-talk is negligible [26,37]. $k^2<(2.5\ \mathrm{km})^2$ is thus a very conservative upper limit, deduced from this criterion.

For ℓ^2, we found that 10% of all data points have $(U_{a,src}/U_{s,src})>1$ for $\ell_\odot^2=(74.0\ \mathrm{km})^2$ and 20% for $\ell_\odot^2=(79.4\ \mathrm{km})^2$.

VI. DISCUSSION AND CONCLUSIONS

New couplings between electromagnetism and gravity introduced within the framework of metric-affine gravity (MAG) theories lead to observable effects, in particular to spacetime becoming birefringent in the presence of a gravitational field. By constraining the level of this birefringence we can constrain the strength of the coupling between electromagnetism and gravity within this particular framework. A birefringence of spacetime is also expected in a more general context, so that such a constraint is also of wider significance.

Using two techniques (the Stokes asymmetry technique and the new profile difference technique applied to solar data) we have imposed stringent constraints on the coupling constant k introduced by MAG. In order to judge how stringent the constraints imposed by these techniques are, we have also redone the analysis for Moffat's NGT. The new techniques improved previous limits on ℓ^2 given by Solanki and Haugan [4] by nearly one order of magnitude. It will be difficult to set much tighter limits on gravitational birefringence than those found here using solar data in the visible spectral range. To obtain a significant improvement one would need to observe at shorter wavelengths. The spectral line at the shortest wavelength that is strong enough to provide a hope of detecting Stokes U and V at sufficient S/N is Lyα at 1216 Å. The maximum gain that one could expect relative to the current analysis is a factor of

$$\frac{\lambda_{\mathrm{visible}}}{\lambda_{\mathrm{Ly}\alpha}}=\frac{5250}{1216}=4.32. \tag{29}$$

Another possibility is to consider astronomical objects with a stronger gravitational field and well defined sources of polarization. In a parallel paper [38] we employ magnetic white dwarfs for this purpose.

[1] R.H. Dicke, *Experimental Relativity*, in *Relativity, Groups and Topology*, edited by C. DeWitt and B. DeWitt (Gordon and Breach, New York, 1964), pp. 165–313.

[2] W.-T. Ni, Phys. Rev. Lett. **38**, 301 (1977).

[3] W.-T. Ni, in *Precision Measurements and Fundamental Constants II*, edited by B.N. Taylor and W.D. Phillips, U.S. National Bureau of Standards Publication 617 (U.S. GPO, Washington, D.C., 1984).

[4] S.K. Solanki and M.P. Haugan, Phys. Rev. D **53**, 997 (1996).

[5] S.K. Solanki, M.P. Haugan, and R.B. Mann, Phys. Rev. D **59**, 047101 (1999).

[6] J.W. Moffat, Phys. Rev. D **19**, 3554 (1979); **19**, 3562 (1979); **35**, 3733 (1987); *Gravitation: A Banff Summer Institute*, edited by R.B. Mann and P. Wesson (World Scientific, Singapore, 1991).

[7] M.D. Gabriel, M.P. Haugan, R.B. Mann, and J.H. Palmer, Phys. Rev. D **43**, 308 (1991).

[8] M.D. Gabriel, M.P. Haugan, R.B. Mann, and J.H. Palmer, Phys. Rev. D **43**, 2465 (1991).

[9] M.D. Gabriel, M.P. Haugan, R.B. Mann, and J.H. Palmer, Phys. Rev. Lett. **67**, 2123 (1991).

[10] M.P. Haugan and T.F. Kauffmann, Phys. Rev. D **52**, 3168 (1995).

[11] T. Damour, S. Deser, and J. McCarthy, Phys. Rev. D **45**, R3289 (1992).

[12] M. Clayton, L. Demopoulos, and J. Legare, Gen. Relativ. Gravit. **30**, 1501 (1998).

[13] F.W. Hehl, J.D. McCrea, E.W. Mielke, and Y. Ne'eman, Phys. Rep. **258**, 1 (1995).

[14] G.F. Rubilar, Y.N. Obukhov, and F.W. Hehl, Class. Quantum Grav. **20**, L185 (2003).

[15] Y. Itin and F.W. Hehl, Phys. Rev. D **68**, 127701 (2003).

[16] R.A. Puntigam, C. Laemmerzahl, and F.W. Hehl, Class. Quantum Grav. **14**, 1347 (1997).

[17] R. Tresguerres, Z. Phys. C **65**, 347 (1995).
[18] R. Tresguerres, Phys. Lett. A **200**, 405 (1995).
[19] A.R. Edmonds, *Angular Momentum in Quantum Mechanics* (Princeton University Press, Princeton, 1974).
[20] S.K. Solanki and J.O. Stenflo, Astron. Astrophys. **140**, 185 (1984).
[21] U. Grossmann-Doerth, M. Schüssler, and S.K. Solanki, Astron. Astrophys. **221**, 338 (1989).
[22] U. Grossmann-Doerth, M. Schüssler, M. Sigwarth, and O. Steiner, Astron. Astrophys. **357**, 351 (2000).
[23] U. Grossmann-Doerth, C.U. Keller, and M. Schüssler, Astron. Astrophys. **315**, 610 (1996).
[24] V. Martínez Pillet, B.W. Lites, and A. Skumanich, Astrophys. J. **474**, 810 (1997).
[25] S.K. Solanki, I. Ruedi, and D. Rabin, Astron. Soc. Pac. **46**, 534 (1993).
[26] J. Sánchez Almeida and B.W. Lites, Astrophys. J. **398**, 359 (1992).
[27] S.R.O. Ploner, M. Schüssler, S.K. Solanki, and A.S. Gadun, in *Advanced Solar Polarimetry—Theory, Observation and Instrumentation, 20th NSO/Sac Summer Workshop, ASP Conference Proceedings Vol. 236*, edited by Michael Sigwarth (Astronomical Society of the Pacific, San Francisco, 2001), p. 363.
[28] H.P. Povel, Opt. Eng. (Bellingham) **34**, 1870 (1995).
[29] S.K. Solanki and J.O. Stenflo, Astron. Astrophys. **170**, 120 (1986).
[30] J. Sánchez Almeida, V. Martínez Pillet, and A.D. Wittmann, Sol. Phys. **134**, 1 (1991).
[31] J. Sánchez Almeida, V. Martínez Pillet, and F. Kneer, Astron. Astrophys. **113**, 359 (1995).
[32] P.N. Bernasconi, Ph.D. Thesis, ETH, Zürich (1997).
[33] A.M. Gandorfer and H.P. Povel, Astron. Astrophys. **328**, 381 (1997).
[34] H.P. Povel, in *Magnetic Fields Across the Hertzsprung-Russell Diagram, ASP Conference Proceedings Vol. 248*, edited by G. Mathys, S. K. Solanki, and D. T. Wickramasinghe (Astronomical Society of the Pacific, San Francisco, 2001).
[35] M. Fligge and S.K. Solanki, *The Tenth Cambridge Workshop on Cool Stars, Stellar Systems and the Sun*, ASP Conf. Ser. 154 (Astronomical Society of the Pacific, San Francisco, 1998), p. 833.
[36] J.O. Stenflo, S.K. Solanki, and J.W. Harvey, Astron. Astrophys. **171**, 305 (1987).
[37] A. Skumanich and B. Lites, Proceedings of the Eleventh National Solar Observatory/Sacramento Peak Summer Workshop, Sunspot, New Mexico, 311 (1990).
[38] O. Preuss, M.P. Haugan, S.K. Solanki, and S. Jordan, An Astronomical Search for Evidence of New Physics, 2003.